

RSC Advances



This is an *Accepted Manuscript*, which has been through the Royal Society of Chemistry peer review process and has been accepted for publication.

Accepted Manuscripts are published online shortly after acceptance, before technical editing, formatting and proof reading. Using this free service, authors can make their results available to the community, in citable form, before we publish the edited article. This *Accepted Manuscript* will be replaced by the edited, formatted and paginated article as soon as this is available.

You can find more information about *Accepted Manuscripts* in the [Information for Authors](#).

Please note that technical editing may introduce minor changes to the text and/or graphics, which may alter content. The journal's standard [Terms & Conditions](#) and the [Ethical guidelines](#) still apply. In no event shall the Royal Society of Chemistry be held responsible for any errors or omissions in this *Accepted Manuscript* or any consequences arising from the use of any information it contains.

Thermal Analysis of Aqueous Urea Ammonium Nitrate Alternative Fuel

Cite this: DOI: 10.1039/x0xx00000x

Alon Grinberg Dana^a, Gennady E. Shter^b, Gideon S. Grader^{b*}

Received 00th January 2014,
Accepted 00th January 2014

DOI: 10.1039/x0xx00000x

www.rsc.org/advances

The thermal decomposition of aqueous ammonium nitrate, aqueous urea and aqueous urea ammonium nitrate was investigated by means of simultaneous TGA/DTA/DTG/MS analysis under ambient pressure, and DSC under applied pressures of 5 and 10 MPa. Aqueous urea ammonium nitrate was previously suggested as a low carbon nitrogen-based alternative fuel. Investigation of the processes which occur in the condensed phase as the temperature increases is crucial in order to understand the combustion mechanism of the suggested alternative fuel. Isomerization of urea into ammonium cyanate as well as urea hydrolysis was inhibited in the presence of ammonium nitrate, hence the fuel is considered to be chemically stable at room temperature. No solid residuals remained above 315 °C. Thermal decomposition of the fuel under ambient pressure was found to involve four principal endothermic stages: (a) water vaporization, (b) urea decomposition along with biuret formation, (c) biuret decomposition, and (d) ammonium nitrate dissociation. The thermal decomposition of the fuel under isobaric conditions of 5 and 10 MPa revealed only an exothermic process with a sharp increase in the heat flow above 300 °C. The present research increases the basic understanding of the suggested nitrogen-based alternative fuel combustion process.

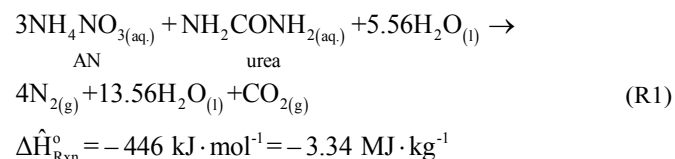
Introduction

Developing a sustainable and secure energy system is perhaps one of the greatest challenges of our society. In particular, the development of carbon-neutral energy storage and energy carrier technologies is a key enabling element for the utilization of energy from renewable intermittent resources (*e.g.*, solar and wind) on demand. Synthesizing chemical fuels is a promising route for large-scale energy storage, since fuels achieve a relatively high energy density through the chemical bonds between light elements (*i.e.*, H-H, C-H, and N-H bonds). In addition, chemical fuels are excellent energy carriers with an existing worldwide distribution infrastructure.

The feasibility of a pure hydrogen economy is questionable due to high costs, safety issues and hydrogen's extremely low volumetric energy density.¹ Practically, hydrogen can be stored *via* two major carriers: carbon and nitrogen. The carbon option requires separation and transport of CO₂ from power plants, which is a tremendous logistic challenge when globally relevant

amounts are considered. However, unlike atmospheric CO₂, the global accessibility to atmospheric nitrogen will enable a large-scale production of ammonia and its fertilizer derivatives, given the availability of abundant hydrogen from future solar water splitting plants.

A low carbon nitrogen-based alternative fuel in the form of an aqueous Urea and Ammonium Nitrate (UAN) solution was previously suggested as an alternative hydrogen carrier.² This nonflammable, nonexplosive and nontoxic fuel can theoretically produce an environmentally friendly effluent gas consisting of 73.0% H₂O, 21.6% N₂, and 5.4% CO₂ (mole basis) upon combustion (Reaction R1). This combustion requires a stoichiometric Ammonium Nitrate (AN) to urea ratio of 3:1 by moles, which is about 4:1 by mass.

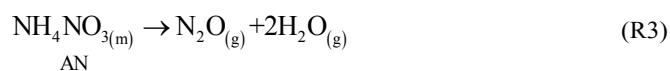
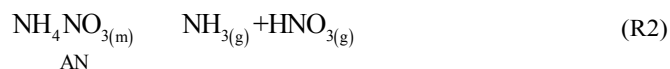


Upon heating, solid AN undergoes multiple phase transitions prior to melting (169.6 °C),³ and dissociates into ammonia and nitric acid (Reaction R2).⁴ An intermolecular proton transfer initiates this endothermic dissociation. Depending on the experimental conditions,⁵⁻⁷ this reaction

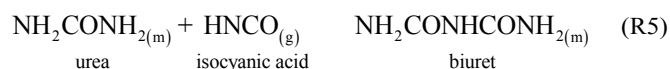
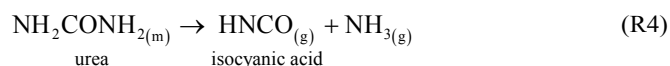
^a The Nancy and Stephen Grand Technion Energy Program, Technion – Israel Institute of Technology, Haifa 3200003, Israel. Fax: +972-77-887-5099.

^b The Wolfson Department of Chemical Engineering, Technion – Israel Institute of Technology, Haifa 3200003, Israel. Fax: +972-4-829-5672, Email: grader@technion.ac.il.

consumes all of the AN at about 250–320 °C. Further reactions between ammonia and nitric acid are reported to proceed *via* an ionic mechanism in the melt,⁸⁻¹⁰ which gradually shifts at higher temperatures to a radical mechanism in the gas phase.⁸ Eventually, both mechanisms lead to the formation of nitrous oxide and water (Reaction R3). Therefore, in a closed system the overall decomposition of AN is exothermic¹¹⁻¹⁴ due to the aforementioned successive gas phase reactions.⁵



The thermal decomposition of solid urea, on the other hand, is surprisingly complex,¹⁵⁻¹⁸ and it is influenced by the crucible's geometry.^{17,19} After melting (133.3 °C),²⁰ urea primarily decomposes into isocyanic acid (HNCO) and NH₃ (Reaction R4).^{21,22} The reactive HNCO undergoes a secondary reaction with the still unreacted urea, forming biuret (Reaction R5).²²⁻²⁴ Larger molecules such as cyanuric acid (CYA), ammelide, ammeline and melamine can also form in the presence of HNCO or NH₃.^{19,20}



Urea is being widely used in diesel NO_x removal processes such as Selective Catalytic Reduction (SCR)^{21,25-27} as an aqueous solution at its eutectic composition (32.5% wt. urea, marketed as AdBlue®).²⁸ Thermal analysis of aqueous urea was previously conducted using a porous monolith impregnated with the solution²⁹ and with a nickel alumina catalyst.¹⁵

Thermal analysis of homogeneous solid UAN (dissolved in distilled water and then dried at 80 °C for 15 min) was previously conducted using a perforated lid screwed to the crucible containing the sample.⁶ Therefore, the evolved gases could react within the crucible, and the overall observed process was exothermic; hence the condensed phase processes were not directly observed. The identified evolved gases were: N₂, H₂O, NO_x, CO₂, NH₃ and HNCO.⁶

Although the separate analysis of urea and AN was previously reported, the thermal analysis of both species in an aqueous solution has never been reported in the current literature. In order to gain a thorough understanding of aqueous UAN combustion mechanism, it is crucial to investigate the processes that occur in the condensed phase which precede the gas phase combustion. Therefore, the main objective of this work is to investigate the chemical processes that aqueous UAN undergoes at elevated temperatures. In this paper, we report on the thermal decomposition of aqueous urea, aqueous

Table 1 Composition of tested samples

Sample	AN (%wt)	Urea (%wt)	Water (%wt)	AN:urea mass ratio
A	50.0%	0%	50.0%	–
B	0%	50.0%	50.0%	–
C1	50.0%	6.25%	43.75%	4:0.5
C2 ^a	50.0%	12.5%	37.5%	4:1
C3	50.0%	18.75%	31.25%	4:1.5
C4	50.0%	25.0%	25.0%	4:2
D1	0%	12.5%	87.5%	–
D2	12.5%	12.5%	75.0%	4:4
D3	25.0%	12.5%	62.5%	4:2
D4 ^a	50.0%	12.5%	37.5%	4:1
E	60.0%	15.0%	25.0%	4:1
P1 (5 MPa)	60.0%	15.0%	25.0%	4:1
P2 (10 MPa)	60.0%	15.0%	25.0%	4:1

^a Samples C2 and D4 represent the same experiment. The samples were given different names for series continuity and presentation clarity.

AN and aqueous UAN solutions at ambient pressure. In addition, we show the typical thermal decomposition of an aqueous UAN solution under applied high pressure. The high pressure experiments (5 MPa and 10 MPa) reported here for the first time resemble the expected conditions during the continuous combustion of the aqueous UAN fuel, since this fuel was reported to yield a relatively low pollutant level above 5 MPa.²

Materials and methods

The samples were prepared using AN (≥99%, Sigma-Aldrich), urea (≥99.5%, Sigma-Aldrich) and water (Milli-Q® ultrapure water). About 70 mg of samples A-E (Table 1) were analyzed by simultaneous Thermal-Gravimetric Analysis and Differential Thermal Analysis (TGA/DTA) at ambient pressure (Setsys Evolution 1750, Setaram). The TGA/DTA measurements were carried out from 25 to 500 °C with a heating rate of 5 °C/min under a 20 ml/min argon flow using a 100 μl alumina crucible. The evolved gases from selected samples were simultaneously analysed by a quadrupole Mass Spectrometer (MS, ThermoStar GSD320, Pfeiffer). Derivative Thermo-Gravimetric (DTG) curves, which represent the rate of mass change, and peak integration were calculated using the Calisto Processing software (AKTS and Setaram).

About 25 mg of samples P1 and P2 (Table 1) were analyzed by a Calvet-type Differential Scanning Calorimetry (DSC, Sensys Evo, Setaram) equipped with 3D heat flow sensors. Therefore, the entire differential heat flow associated with all processes, both in the condensed and in the gas phases, was detected. The DSC examinations were carried out from 25 to 500 °C with a heating rate of 5 °C/min in an isobaric system under 5 MPa and 10 MPa initially applied by nitrogen.

Results and discussion

Aqueous AN

Fig. 1 presents the TGA/DTA/DTG curves of an aqueous AN solution (Sample A). The aqueous AN decomposition

thermogram was divided into three stages. Only endothermic effects were observed without any residual mass above 310 °C. The endothermic process in stage S1 is attributed to water vaporization. Melting of AN was observed at 173 °C (slightly above the theoretical value) only as a minor endotherm, since precipitation of the solid AN phase was incomplete due to the presence of residual water. At the AN melting point about 48.3% of the initial sample mass was lost due to water vaporization. Immediately upon melting, AN dissociation (Reaction R2) commenced, as evident from the DTG (Fig. 1).

Although small amounts of water are required to initiate the AN dissociation,³⁰ the presence of water inhibits AN decomposition.^{8,9} Subsequent to water vaporization, two distinct endotherms were observed, denoted as stages S2 and S3 (Fig. 1). These endotherms are associated with the ionic and radical AN decomposition mechanisms,⁸ respectively.

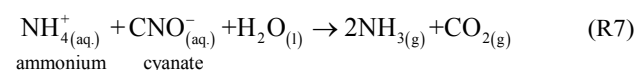
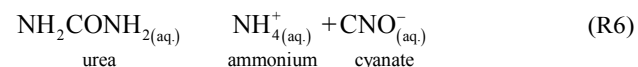
Several reactions in the ionic mechanism, which is dominant at the lower temperature range, were inhibited by the residual water. As the water continued to vaporize, the reactions between the accumulated ions in the melt proceeded, giving rise to the endotherm in stage S2.

Simultaneously, the rate of the radical mechanism, specifically homolysis of HNO₃ as the rate determining step,⁸ increased and the radical mechanism became dominant in stage S3. The endotherm in stage S3 is attributed to AN dissociation (Reaction R2) coupled with HNO₃ homolysis into OH and NO₂ radicals.¹² Exothermic gas phase reactions could also affect the shape of this endotherm. During stage S3, *i.e.* above 230 °C, about 47.5% of the initial sample mass was consumed.

Aqueous urea

Fig. 2 presents the TGA/DTA/DTG curves of an aqueous urea solution (Sample B), coupled with MS curves of the evolved gaseous species. The aqueous urea decomposition thermogram was divided into six stages. Only endothermic effects were observed, and a mass residual of 1.6% remained at 500 °C.

Water vaporization was affected by the dissolved urea.³¹⁻³³ The vaporization was accompanied by a significant mass loss of about 40% (Fig. 2A), and water vapor were detected by the MS (Fig. 2B). In addition, CO₂ and NH₃ were also detected in this temperature range. Aqueous urea is known to be in equilibrium with its isomer ammonium cyanate (Reaction R6).³⁴⁻³⁸ Therefore, the detected CO₂ and NH₃ could have evolved from hydrolysis of ammonium cyanate (Reaction R7).



Alternatively, hydrolysis of the cyanate ion could yield bicarbonate ions (Reaction R8)^{32,39} or ammonium carbonate,^{39,44} either of which could react with ammonium ions to form CO₂, NH₃, and water (Reactions R9, R10).^{41,42} Equilibrium between cyanate and bicarbonate could consume as much as 30% of the cyanate.³⁴

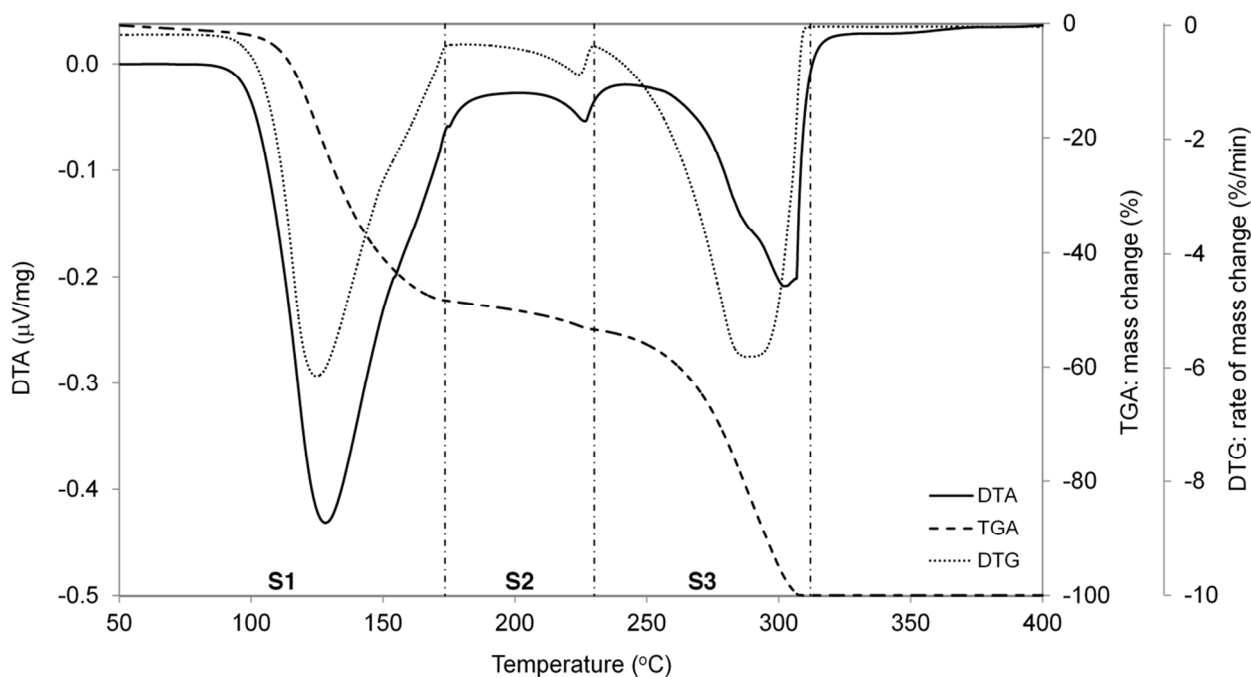


Fig. 1 Thermal analysis of an aqueous AN solution (Sample A) under a 20 ml/min flow of Ar and a heating rate of 5 °C/min. DTA, TGA and calculated DTG curves are presented as a function of the sample temperature. The range between two consecutive vertical dashed lines represents a process stage (denoted as S1-S3). Stages were selected according to major DTG peaks.

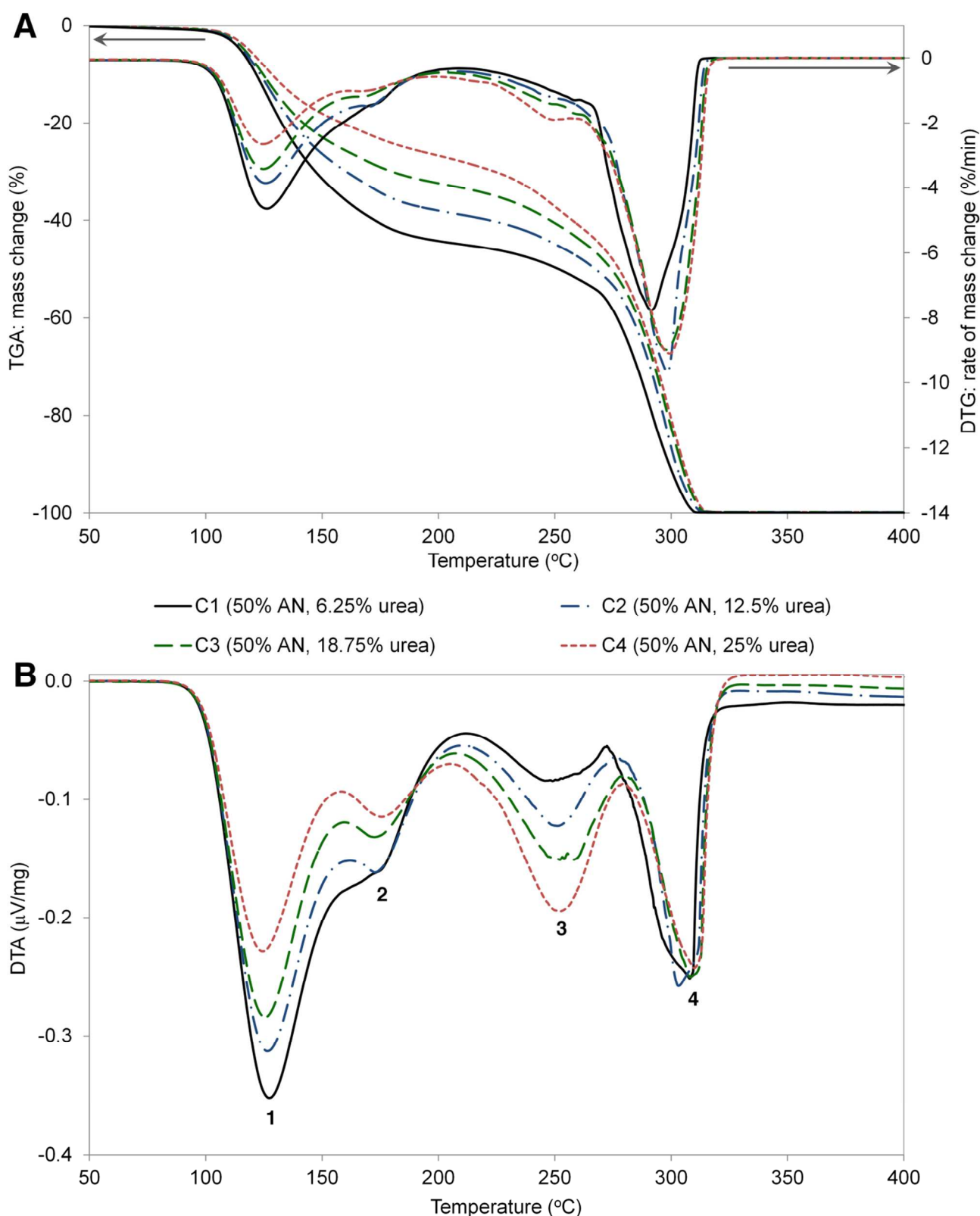


Fig. 3 Thermal analysis of aqueous UAN solutions with a constant AN concentration (Samples C1-C4) under a 20 ml/min flow of Ar and a heating rate of 5 °C/min. (A) TGA/DTG curves. (B) DTA curves. Peaks are numbered for comparison of peak area.

losses. These endotherms correspond to melting and partial decomposition of ammelide and ammeline at about 400 °C,

and 435 °C, respectively. Ammelide and ammeline are reported to completely decompose at temperatures slightly

higher than 600 °C and 700 °C, respectively.²⁰

Effect of AN:urea ratio

Thermal analysis of aqueous UAN solutions with a constant AN concentration was conducted in order to associate each thermolysis stage with its principal reactants. Samples C1-C4 in this series consist of AN at a constant concentration of 50.0%, urea at a varying concentration of 6.25%, 12.5%, 18.75%, and 25.0%, and water as the balance (Table 1). The thermal analysis presented in Fig. 3A revealed a complete mass loss below 315 °C for all the samples in this series.

Based on the DTA data (Fig. 3B), a quantitative comparison between the endothermic signal intensities for different samples in this series was conducted by integrating the respective peak areas, as presented in Table 2. These calculated values represent the relative effect of similar processes which take place at similar temperature ranges.

The first endothermic process detected by DTA (T_{onset} at about 80 °C) is attributed to water vaporization (denoted as 1 in Fig. 3B). The intensity of this endotherm decreased (Table 2), and the mass change was respectively lower (Fig. 3A) as the water concentration decreased (Table 1).

The endothermic effects of the two following processes (denoted as 2 and 3 in Fig. 3B) were significantly more intense as the urea concentration increased (Table 2). These processes are therefore primarily associated with reacting urea or urea derivatives.

The fourth and final thermal stage in this series (denoted as 4 in Fig. 3B) is strongly endothermic. The slight variation in the measured peak area (Table 2) could be explained due to overlapping between peaks 3 and 4. Higher urea concentrations increased the area of peak 3, and the onset temperature of peak 4 (at about 280 °C) appeared slightly shifted to the right. As a consequence, the area of the latter seems to decrease at higher urea concentrations (Table 2). If these peaks were not superimposed, peak 4 would seem indifferent to variations in the urea concentration in terms of intensity and temperature range. Therefore, we conclude that this stage is primarily associated with decomposition of AN, which was at a constant concentration throughout this series.

The analogous thermal analysis of aqueous UAN solutions with a constant urea concentration is presented in Fig. 4. Samples D1-D4 in this series consist of AN at a varying concentration of 0%, 12.5%, 25.0%, and 50.0%, urea at a constant concentration of 12.5%, and water as the balance (Table 1).

Table 2 Comparison of peak areas as denoted in Fig. 3 (units are in $\mu\text{V}\cdot\text{s}\cdot\text{mg}^{-1}$)

Sample	Area of peak 1	Area of peak 2	Area of peak 3	Area of peak 4
C1	84.9	4.6	12.7	58.8
C2	82.2	6.2	22.0	54.1
C3	76.3	7.0	32.7	49.7
C4	61.7	8.0	45.5	49.8

Samples D1 and B consist of aqueous urea at different concentrations of 12.5% and 50.0%, respectively (Table 1). The thermogram of Sample B was thoroughly described above, and, overall, the thermogram patterns of both samples are similar.

The DTA and TGA signals related to urea decomposition and subsequent formation of biuret (Reaction R14) in the temperature range of 190–250 °C are smaller in Sample D1 (Fig. 4) compared to Sample B (Fig. 2). Likewise, decomposition of CYA (Reaction R23) in the temperature range of 310–390 °C was observed in Sample D1 as minor endothermic effect and mass loss in comparison to Sample B.

On the other hand, in the temperature range of 150–170 °C, the endothermic effect attributed to urea hydrolysis (Reaction R11-R12) was found to be larger in Sample D1 than in the more concentrated Sample B. This phenomenon coincides with the reported acceleration of urea hydrolysis by excess of water.⁴⁶ The water:urea mole ratio at the beginning of hydrolysis can be obtained from the TGA data and the molar masses. This ratio was calculated to be about 7.33:1 and 0.67:1 with regard to Samples D1 and B, respectively. In other words, during the hydrolysis water was in excess in Samples D1 and in deficiency in Sample B.

The peak representing urea hydrolysis was also detected in Sample D2 (Fig. 4), though to a lesser extent than in Sample D1. As the AN concentration increased, urea hydrolysis was inhibited. This can be explained by the joint effect of the decrease in water content and the increase in ammonium (NH_4^+) ions in the system, which shifted the hydrolysis equilibrium mediated by the formation of ammonium carbamate (Reaction R11) to the left, according to *Le Chatelier's* principle. The DTA/DTG curves confirm the lower extent of hydrolysis in Sample D2 (Fig. 4).

Likewise, several solutes,³⁵ specifically ammonium ions,^{34,38} are reported to shift the equilibrium between urea and ammonium cyanate (Reaction R6) towards urea. As a result, urea was more stable in its aqueous form up to about 160 °C in the presence of AN. Therefore, considerably more urea decomposed (Reaction R4) at the next stage, and subsequently formed biuret (Reaction R5). This decomposition was observed as an endothermic peak in the thermogram of Sample D4 in the wider temperature range of 160–205 °C (Fig. 4B).

The endotherms of Samples D2-D4 in the temperature range of 250–320 °C (Fig. 4B) are attributed mainly to AN dissociation into NH_3 and HNO_3 (Reaction R2). The mass losses during the dissociation are in accordance with the initial AN mass in each sample: 12.1%, 24.4%, and 49.1% with regard to Samples D2-D4, respectively. In fact, these numbers are slightly lower than the initial AN mass, since AN dissociation initiated prior to this temperature range, as established above (Fig. 1).

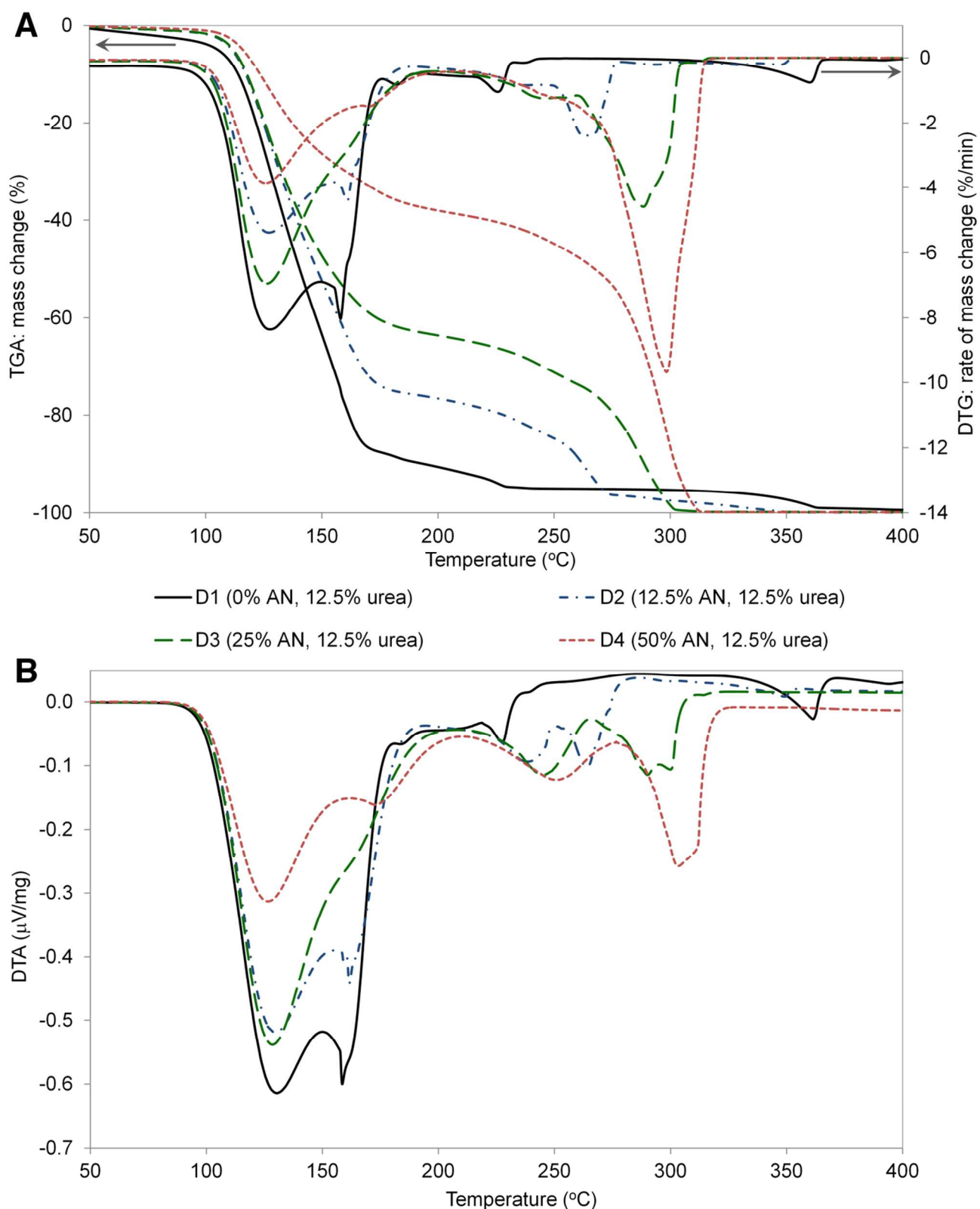


Fig. 4 Thermal analysis of aqueous UAN solutions with a constant urea concentration (Samples D1-D4) under a 20 ml/min flow of Ar and a heating rate of 5 °C/min. (A) TGA/DTG curves. (B) DTA curves.

Decreased CYA formation with increasing AN concentrations is evident in two manners. First, the

endotherm representing CYA decomposition in the temperature range of 290–360 °C was less intense as the AN

concentration increased; this can be seen in particular by comparing the thermograms of Samples D1 and D2 (Fig. 4B). Decomposition of CYA was not observed during the thermolysis of Sample D4 due to an overlap with the dominant AN dissociation effect (Fig. 4). Secondly, the peak in the temperature range of 205–270 °C transformed from relatively sharp (Sample D1) to wider and more intense (Sample D4) as the AN concentration increased (Fig. 4B). This implies that biuret decomposed (Reactions R19, R4) instead of forming CYA (Reaction R15) as the AN concentration increased.

The mass residual at 400 °C was also affected by the increasing AN concentration in these solutions (Fig. 4A). As described earlier, ammeline and melamine are primarily formed by reactions with trapped NH₃ in the solid CYA matrix (Reactions R21–R22). The DTA curve of Sample D1 at about 240 °C (Fig. 4B) is associated with these reactions. This explains the mass residual of about 0.3% at 400 °C with regard to this sample. However, in the presence of AN, the solid CYA matrix, which entraps NH₃ and HNCO, did not evolve, or diminished prematurely, thus no ammeline or melamine residuals formed. As a consequence, no significant mass residual was observed with regard to Samples D2–D4 at 400 °C.

Aqueous UAN

Fig. 5 presents the TGA/DTA/DTG curves of a stoichiometric (according to Reaction R1) near saturation aqueous UAN solution (Sample E), coupled with MS curves of the evolved gaseous species. The aqueous UAN decomposition thermogram was divided into four stages. Only endothermic effects were observed along with a complete mass loss below 315 °C. Table 3 presents the processes that occurred in the condensed phase during thermal decomposition, along with a comparison between the theoretical and experimental mass changes at each stage.

The endotherm in stage S1 is attributed to water vaporization as evident by the MS water signal (Fig. 5). In fact, only 75% of the water has been vaporized during this stage, and vaporization was completed in stage S2. During stage S1 no significant rise in the NH₃ MS signal was

detected (Fig. 5B), unlike the analysis of the aqueous urea solution (Fig. 2B). This implies that during thermal decomposition of aqueous UAN the conversion of urea into ammonium cyanate (Reaction R6) is insignificant. The reason for this phenomenon was discussed above.

The endotherm in stage S2 represents urea decomposition and consecutive formation of biuret (Reaction R14). The mass loss in stage S2, in addition to water vaporization, is a result of NH₃ outflow during Reaction R14 which theoretically amounts to about 2.1% of the initial mass. The experimental mass loss during stages S1 and S2 was found to be slightly lower than the sum of the water content in the solution (25%) and the expected NH₃ outflow (Table 3). This could be due to dissolved NH₃ or perhaps residual water in the melt. Some NO_x were also detected in stage S2 (Fig. 5B), presumably due to slight decomposition of AN *via* the ionic mechanism.

During stage S3 biuret decomposed into NH₃ and HNCO (Reactions R19, R4). Gas phase reaction of HNCO with H₂O formed CO₂ (Reaction R13), as detected by MS (Fig. 5B). During this stage biuret could have also formed small amounts of CYA.

Gradual endothermic AN dissociation into NH₃ and HNO₃ (Reaction R2) began subsequently to its melting point (169.6 °C), and occurred mainly during stage S4, as seen in the DTA/TGA/DTG curves, along with an increasing HNO₃ signal (Fig. 5). Since the dissociation began prior to 270 °C, the experimental mass loss during stage S4 was expected to be slightly lower than the theoretical value of 60%. The slightly higher mass loss deviation from the theoretical value can be explained by a small CYA amount which was formed during stage S3, and decompose simultaneously with AN during stage S4 (Table 3). Decomposition of CYA (Reaction R23) in stage S4 is consistent with the observed HNCO signal (Fig. 5B).

The m/z=30 signal is dominant in the MS spectrum of NO₂, NO, and N₂O,⁴⁸ and is defined herein as NO_x. During stage S4 NO_x, N₂, and H₂O were also observed (Fig. 5B). The presence of these species suggests that exothermic gas phase reactions between the dissociation products of AN, namely HNO₃ and NH₃, took place above the crucible.³

Table 3 The condensed phase processes of aqueous UAN during thermal decomposition

Stage	Temperature range (°C)	Δm (experimental)	Δm (theory)	Process
S1	83 – 156	- 18.6%	- 25.0% + α ^a	H ₂ O _(l) → H ₂ O _(g) ↑
S2	156 – 210	- 8.0%	- 2.1% - α ^a	H ₂ O _(l) → H ₂ O _(g) ↑ urea → HNCO + NH ₃ ↑ urea + HNCO → biuret
S1+S2	83 – 210	- 26.6%	- 27.1%	-
S3	210 – 269	- 12.8%	- 12.9%	biuret → NH ₃ ↑ + 2HNCO ↑
S4	269 – 315	- 60.6%	- 60.0%	AN → HNO ₃ ↑ + NH ₃ ↑

^a Sample mass percentage attributed to water which did not evaporate in Stage S1 is represented by α.

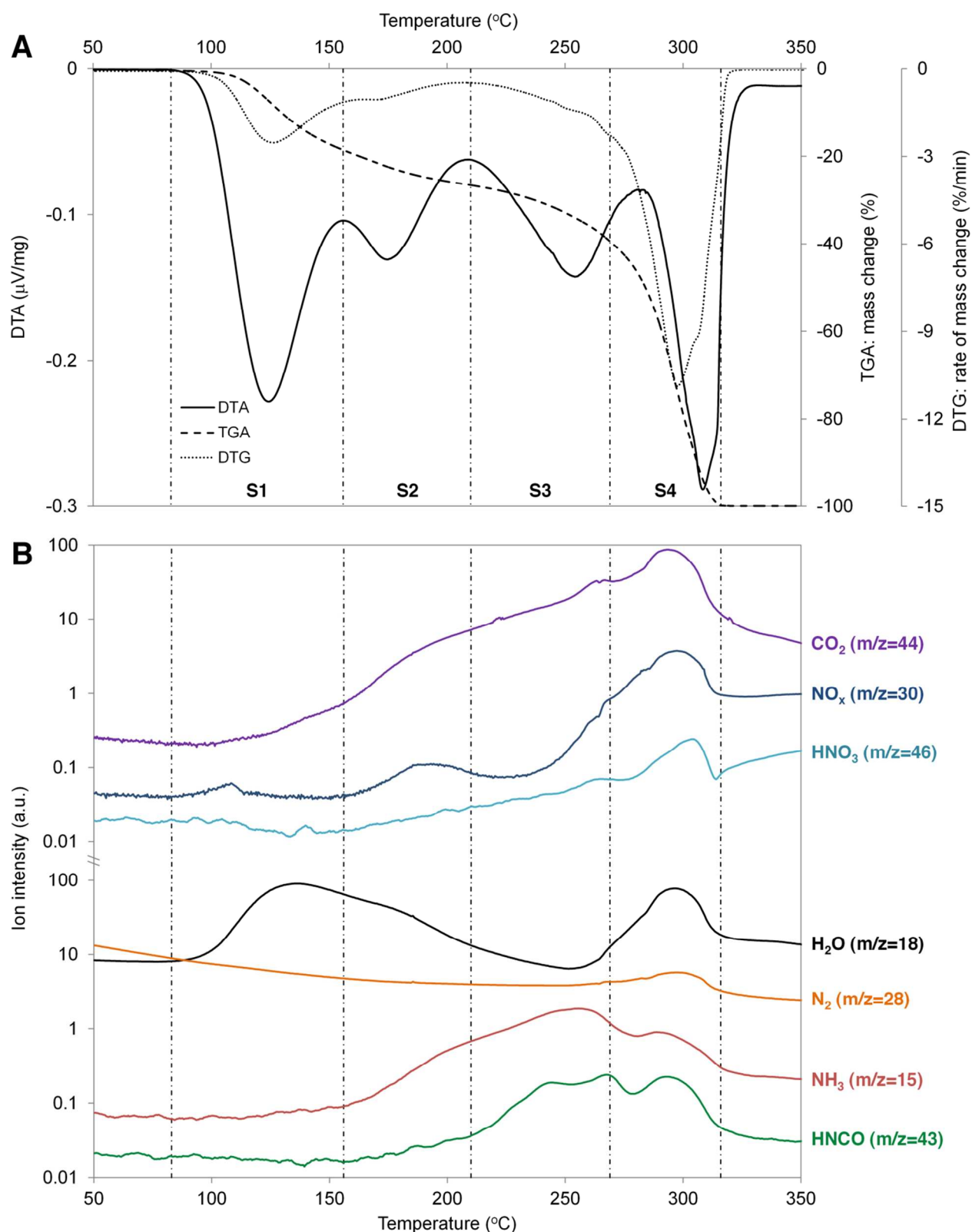


Fig. 5 Thermal analysis with evolved gas analysis of an aqueous UAN solution with a stoichiometric AN:urea ratio (Sample E) under a 20 ml/min flow of Ar and a heating rate of 5 $^{\circ}\text{C}/\text{min}$. The range between two consecutive vertical dashed lines represents a process stage (denoted as S1-S4). Stages were selected according to major DTG peaks. (A) TGA/DTA/DTG curves. (B) Evolved gases detected by MS.

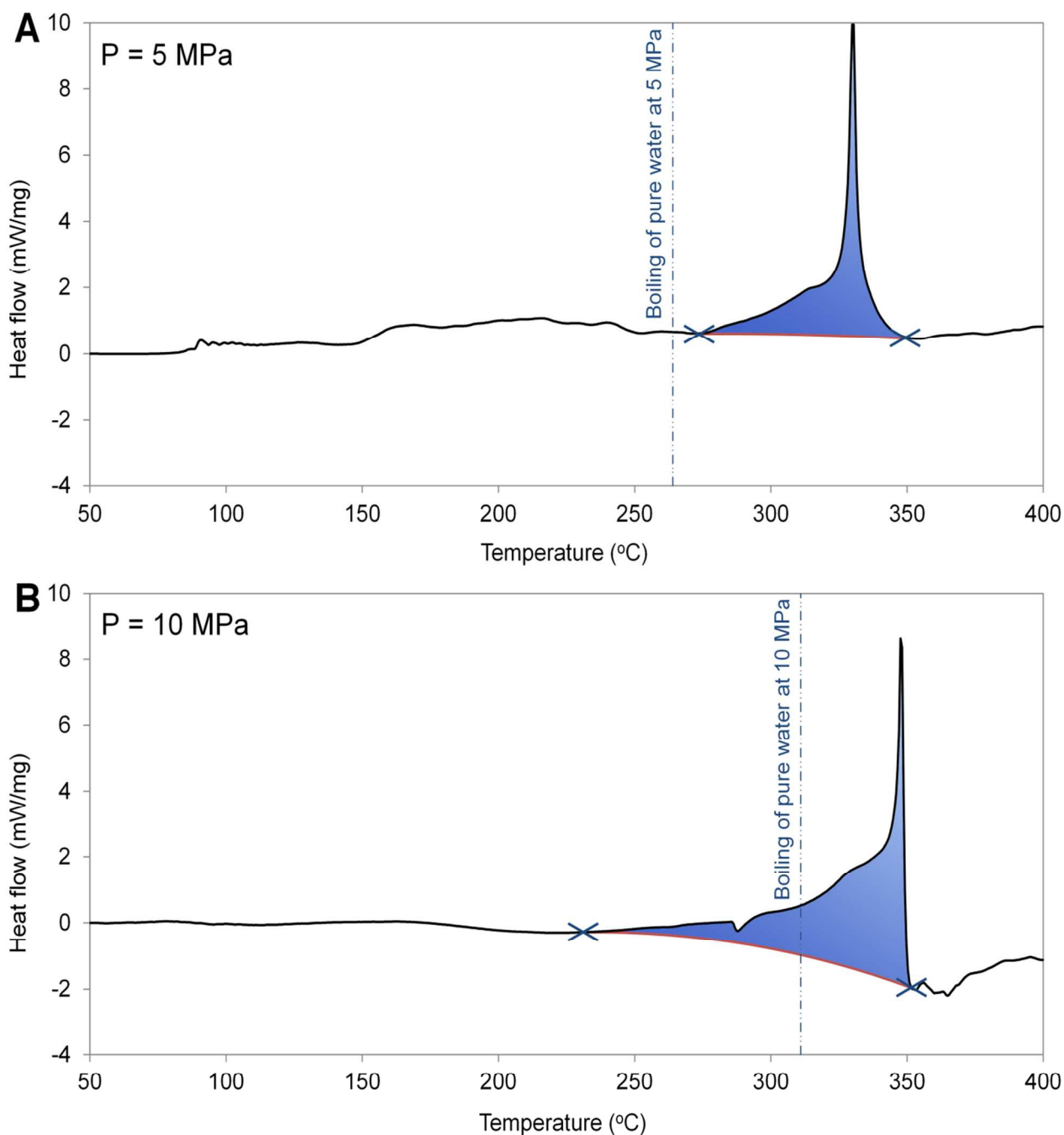


Fig. 6 DSC curves of aqueous UAN solutions with a stoichiometric AN:urea ratio (Samples P1, P2) at a heating rate of 5 °C/min, initially pressurized with N₂. Boiling point of pure water at each pressure is represented by a vertical dashed line. The analysis was conducted under constant pressures of (A) 5 MPa, and (B) 10 MPa.

DSC analysis under applied pressure

The continuous combustion of the aqueous UAN fuel was reported to yield relatively low levels of pollutants at pressures higher than 5 MPa.² As a consequence, thermal analysis of aqueous UAN combustion under high pressures is of great interest. Therefore, isobaric calorimetric experiments were conducted under 5 and 10 MPa (Samples P1 and P2, Table 1).

In this series, the nature of the thermal processes changed dramatically in comparison with the processes under ambient pressure (Fig. 5A). As presented in Fig. 6, under the applied pressure both thermograms exhibited a strong exotherm with a sharp increase of heat flow above 300 °C. The peak maximum, which is the temperature at which the reaction rate is highest, shifted to a higher temperature from 330 °C to about 350 °C as the pressure increased from 5 MPa to 10 MPa. On the other hand, the

onset of the detectable exothermic effect shifted towards a lower temperature from 270 °C to 220 °C.

At 5 MPa and 10 MPa the boiling temperatures of pure water are 264 °C and 311 °C, respectively.⁵³ In the presence of UAN, water vaporization extends above the boiling temperature of pure water. For example, in an aqueous UAN solution under ambient pressure and a 5 °C/min heating rate, although the water vaporization initiated slightly below the boiling temperature of pure water (100 °C), it extended over a temperature range of about 30 °C (Fig. 5A). The water vaporization endotherm was not observed directly in the experiment series conducted under applied high pressure, probably since it was superimposed with the dominant exothermic reactions. In addition, since AN decomposition is inhibited by water, as previously validated up to 275 °C,⁹ the increase in the water boiling point temperature resulted in a shift of the peak maximum towards higher temperatures.

Furthermore, two additional endothermic effects associated with urea and biuret decomposition (S2 and S3 in Table 3) which were observed under ambient pressure (Fig. 5A) were not detected under the applied high pressures (Fig. 6). This could be due to the presence of water in a wider temperature range due to the increased boiling temperature, and due to the stabilization effect of urea by water.⁵⁴ Since urea decomposition was insignificant prior to the onset temperature of the exothermic reactions, only minor amounts of biuret might have formed under these conditions; hence biuret decomposition peak was insignificant as well, and was not observed.

The exothermic effect under both examined high pressures consisted of a moderate increase followed by a sharp increase in the heat flow (Fig. 6). According to the boiling temperature of pure water at each pressure, the water was in the liquid phase at the beginning of the observed exothermic effect. Therefore, the exothermic reactions began in the liquid UAN phase. These reactions could be redox reactions between AN and urea or between AN dissociation products. Once the water vaporized, and a sufficient reactant concentration in the gas phase was achieved, exothermic gas phase reactions commenced as a volume thermal explosion, observed as a sharp increase in the heat flow. The initial reactants in the gas phase are assumed to be NH₃, HNO₃ and HNCO.

It is thus emphasized that these gas phase reactions observed by the high pressure DSC could not have occurred in an open system under ambient pressure and gas flow. Water vaporization occurs at a relatively low temperature under ambient pressure, hence the unstabilized urea decomposes prematurely and the HNCO gas exits the system ill-timed. Dissociation products of AN (Reaction R2) also escape the system before a sufficient gas phase concentration is established to sustain the thermal combustion reactions.

Conclusions

Thermal analysis of aqueous AN, aqueous urea, and aqueous UAN at several concentrations was conducted under ambient pressure. Thermal analysis of aqueous UAN was conducted under constant pressures of 5 and 10 MPa. In addition, evolved gas analysis of aqueous urea and stoichiometric aqueous UAN solutions was conducted.

Aqueous AN was found to decompose above AN's melting point *via* two consecutive mechanisms, consistent with the literature. The first mechanism involves an ionic reaction pathway and the second one involves a radical reaction pathway.

Urea was in equilibrium with ammonium cyanate in an aqueous solution at room temperature, and both species hydrolyzed during heating. Thermal decomposition of urea resulted in the formation of biuret, CYA, and other large molecules (ammelide, ammeline and melamine), some of which remained as solid residues at 500 °C.

Thermal analysis of aqueous UAN series showed that urea conversion into ammonium cyanate and urea hydrolysis were inhibited as the concentration of AN increased. Consequently, at relatively high AN concentrations the urea was available to decompose and subsequently oxidize, rather than hydrolyze. Furthermore, the aqueous UAN fuel is considered to be chemically stable at room temperature, containing no other species in a significant concentration in addition to AN, urea, and water. Moreover, no mass residues persisted above 315 °C during the thermal decomposition of the fuel, unlike the thermal decomposition of aqueous urea.

Thermal analysis of aqueous UAN with a stoichiometric AN:urea mass ratio of 4:1 revealed four endothermic stages which were identified as: (a) water vaporization, (b) urea decomposition coupled with biuret formation, (c) biuret decomposition, and (d) AN dissociation. The observed mass losses and detected evolved gases were in agreement with these stages. The absence of exothermic effects suggests that under ambient pressure the suggested aqueous fuel is safe to handle, store and transport.

The pressure had a significant effect on the thermal processes. DSC analysis of a stoichiometric aqueous UAN solution in an isobaric system under 5 and 10 MPa revealed a wide exothermic effect with a sudden increase in the measured heat flow above 300 °C. The absence of endothermic effects, specifically up to 250 °C, suggests that no detectable amounts of biuret, CYA, or other urea derivatives were formed at these conditions. Under the applied high pressures, the exothermic reactions began in the condensed phase. Subsequent to water vaporization, the exothermic reactions advanced in the gas phase by a radical volume thermal explosion mechanism.

The present research highlights the chemical processes which occur in the reacting condensed phase of the aqueous UAN nitrogen-based fuel, and sets the stage for an in-depth investigation of the chemical combustion mechanism of this fuel.

Acknowledgements

The authors acknowledge the generous support of Mr. Ed Satell, Philadelphia, PA, and the Nancy and Stephen Grand Technion Energy Program (GTEP), as well as the Committee for Planning and Budgeting of the Council for Higher Education under the framework of the KAMEA Program. The authors acknowledge the assistance of Setaram Instrumentations, France, in conducting the DSC experimentation.

Notes and references

- Committee on Alternatives and Strategies for Future Hydrogen Production and Use, National Research Council, National Academy of Engineering, in *The Hydrogen Economy: Opportunities, Costs, Barriers, and R&D Needs*, The National Academies Press, Washington, D.C., 2004, ISBN: 978-0309530682.
- A. Grinberg Dana, G. E. Shter, G. S. Grader, *RSC Adv.*, 2014, **4**(20), 10051-10059, DOI: 10.1039/c3ra47890d.
- L. A. Medard, in *Accidental Explosions*, Wiley, Chichester, England, 1989, vol. 2, ch. 23, ISBN: 978-0470215326.
- H. L. Saunders, *J. Chem. Soc., Trans.*, 1922, **121**, 698-711, DOI: 10.1039/ct9222100698.
- R. Gunawan, D. Zhang, *J. Hazard. Mater.*, 2009, **165**, 751-758, DOI: 10.1016/j.jhazmat.2008.10.054.
- S. Biamino, C. Badini, *J. Eur. Ceram. Soc.*, 2004, **24**, 3021-3034, DOI: 10.1016/j.jeurceramsoc.2003.10.005.
- S. Chaturvedi, P. N. Dave, *J. Energ. Mater.*, 2013, **31**(1), 1-26, DOI: 10.1080/07370652.2011.573523.
- K. R. Brower, J. C. Oxley, M. Tewari, *J. Phys. Chem.*, 1989, **93**(10), 4029-4033, DOI: 10.1021/j100347a033.
- W. A. Rosser, S. H. Inami, H. Wise, *J. Phys. Chem.*, 1963, **67**(9), 1753-1757, DOI: 10.1021/j100803a004.
- B. J. Wood, H. Wise, *J. Chem. Phys.*, 1955, **23**, 693-696, DOI: 10.1063/1.1742078.
- J. C. Oxley, J. L. Smith, E. Rogers, M. Yu, *Thermochim. Acta*, 2002, **384**, 23-45, DOI: 10.1016/S0040-6031(01)00775-4.
- D. E. G. Jones, H. Feng, K. J. Mintz, R. A. Augsten, *Thermochim. Acta*, 1999, **331**(1), 37-44, DOI: 10.1016/S0040-6031(98)00660-1.
- D. E. G. Jones, P. Handa, H. Feng, *J. Therm. Anal. Calorim.*, 1998, **53**(1), 3-10, DOI: 10.1023/a:1010100504084.
- J. Sun, Z. Sun, Q. Wang, H. Ding, T. Wang, C. Jiang, *J. Hazard. Mater.*, 2005, **127**, 204-210, DOI: 10.1016/j.jhazmat.2005.07.028.
- J. M. Jones, A. N. Rollinson, *Thermochim. Acta*, 2013, **565**, 39-45, DOI: 10.1016/j.tca.2013.04.034.
- M. Koebel, E. O. Strutz, *Ind. Eng. Chem. Res.*, 2003, **42**, 2093-2100, DOI: 10.1021/ie020950o.
- A. G. Koryakin, V. A. Gal'perin, A. N. Sarbaev, A. I. Finkel'shtein, *Zh. Org. Khim.*, 1971, **7**, 989-994.
- W. Brack, B. Heine, F. Birkhold, M. Kruse, G. Schoch, S. Tischer, O. Deutschmann, *Chem. Eng. Sci.*, 2014, **106**, 1-8, DOI: 10.1016/j.ces.2013.11.013.
- M. Eichelbaum, R. J. Farrauto, M. J. Castaldi, *Appl. Catal., B*, 2010, **97**(1-2), 90-97, DOI: 10.1016/j.apcatb.2010.03.027.
- P. M. Schaber, J. Colson, S. Higgins, D. Thielen, B. Anspach, J. Brauer, *Thermochim. Acta*, 2004, **424**, 131-142, DOI: 10.1016/j.tca.2004.05.018.
- M. Koebel, M. Elsener, M. Kleemann, *Catal. Today*, 2000, **59**(3-4), 335-345, DOI: 10.1016/S0920-5861(00)00299-6.
- S. Sebelius, T. T. Le, L. J. Pettersson, H. Lind, *Chem. Eng. J.*, 2013, **231**, 220-226, DOI: 10.1016/j.cej.2013.06.124.
- P. J. C. Kaasenbrood, P. J. Van Den Berg, L. J. Revallier, *J. Agric. Food Chem.*, 1963, **11**(1), 39-43, DOI: 10.1021/jf60125a012.
- C. E. Redemann, F. C. Riesenfeld, F. S. La. Viola, *Ind. Eng. Chem.*, 1958, **50**(4), 633-636, DOI: 10.1021/ie50580a035.
- H. L. Fang, H. F. M. DaCosta, *Appl. Catal., B*, 2003, **46**(1), 17-34, DOI: 10.1016/S0926-3373(03)00177-2.
- S. D. Yim, S. J. Kim, J. H. Baik, I. S. Nam, Y. S. Mok, J. H. Lee, B. K. Cho, S. H. Oh, *Ind. Eng. Chem. Res.*, 2004, **43**(16), 4856-4863, DOI: 10.1021/ie034052j.
- C. S. Sluder, J. M. E. Storey, S. A. Lewis, L. A. Lewis, SAE Technical Paper 2005-01-1858, 2005, DOI: 10.4271/2005-01-1858.
- AUS32 (AdBlue®) Specifications as per ISO22241, <http://www.iso22241.org/>, (accessed April 2014).
- A. Lundström, B. Andersson, L. Olsson, *Chem. Eng. J.*, 2009, **150**(2-3), 544-550, DOI: 10.1016/j.cej.2009.03.044.
- L. Friedman, J. Bigeleisen, *J. Chem. Phys.*, 1950, **18**, 1325-1331, DOI: 10.1063/1.1747471.
- F. Birkhold, U. Meingast, P. Wassermann, O. Deutschmann, *Appl. Catal., B*, 2007, **70**, 119-127, DOI: 10.1016/j.apcatb.2005.12.035.
- V. Ebrahimi, A. Nicolle, C. Habchi, *AIChE J.*, 2012, **58**(7), 1998-2009, DOI: 10.1002/aic.12736.
- S. Kontin, A. Höfler, R. Koch, H. J. Bauer, 23rd Annual Conference on Liquid Atomization and Spray Systems, Brno, 2010.
- J. Shorter, *Chem. Soc. Rev.*, 1978, **7**, 1-14, DOI: 10.1039/CS9780700001.
- J. C. Warner, F. B. Stitt, *J. Am. Chem. Soc.*, 1933, **55**(12), 4807-4812, DOI: 10.1021/ja01339a010.
- P. Dirnhuber, F. Schütz, *Biochem. J.*, 1948, **42**(4), 628-632.
- A. N. Alexandrova, W. L. Jorgensen, *J. Phys. Chem. B*, 2007, **111**(4), 720-730, DOI: 10.1021/jp066478s.
- J. Walker, F. J. Hambly, *J. Chem. Soc., Trans.*, 1895, **67**, 746-767, DOI: 10.1039/CT8956700746.
- P. A. H. Wyatt, H. L. Kornberg, *Trans. Faraday Soc.*, 1952, **48**, 454-462, DOI: 10.1039/TF9524800454.
- A. H. England, A. M. Duffin, C. P. Schwartz, J. S. Uejio, D. Prendergast, R. J. Saykally, *Chem. Phys. Lett.*, 2011, **514**, 187-195, DOI: 10.1016/j.cplett.2011.08.063.
- P. Nowak, J. Skrzypek, *Chem. Eng. Sci.*, 1989, **44**(10), 2375-2377, DOI: 10.1016/0009-2509(89)85170-x.
- K. G. Clark, V. L. Gaddy, C. E. Rist, *Ind. Eng. Chem.*, 1933, **25**(10), 1092-1096, DOI: 10.1021/ie50286a008.
- G. Estiu, K. M. Merz, *J. Phys. Chem. B*, 2007, **111**(23), 6507-6519, DOI: 10.1021/jp0677086.

- 44 M. Yao, W. Tu, X. Chen, C. G. Zhan, *Org. Biomol. Chem.*, 2013, **11**, 7595-7605, DOI: 10.1039/C3OB41055B.
- 45 R. C. Warner, *J. Biol. Chem.*, 1942, **142**, 705-723.
- 46 H. B. H. Cooper, H. W. Spencer III, *US Pat.*, 6 077 491, 2000.
- 47 J. Sahu, K. Mahalik, A. Patwardhan, B. Meikap, *Ind. Eng. Chem. Res.*, 2008, **47**(14), 4689-4696, DOI: 10.1021/ie800481z.
- 48 The NIST Chemistry WebBook, <http://webbook.nist.gov/>, (accessed April 2014).
- 49 NIST Chemical Kinetics Database, <http://kinetics.nist.gov/>, (accessed April 2014).
- 50 Z. C. Chen, W. J. Yang, J. H. Zhou, H. K. Lv, J. Z. Liu, K. F. Cen, *J. Zhejiang Univ. Sci. A*, 2010, **11**(11), 849-856, DOI: 10.1631/jzus.A0900798.
- 51 H. Kinoshita, *RvPCJ*, 1955, **25**(1), 34-37, HDL: 2433/46723.
- 52 K. Huthmacher, D. Most, in *Cyanuric acid and Cyanuric chloride*, Ullmann's Encyclopedia of Industrial Chemistry, 2000, DOI: 10.1002/14356007.a08_191.
- 53 NIST-JANAF Thermochemical Tables, <http://kinetics.nist.gov/janaf/>, (accessed April 2014).
- 54 M. C. Stumpe, H. Grubmüller, *J. Phys. Chem. B*, 2007, **111**, 6220-6228, DOI: 10.1021/jp066474n.